Ceramics International xxx (xxxx) xxx–xxx

Contents lists available at ScienceDirect

Ceramics International

journal homepage: www.elsevier.com/locate/ceramint

Crystal structure, infrared spectra and microwave dielectric properties of a novel low-firing $Gd_2Zr_3(MoO_4)_9$ ceramic

C.F. Xing, B. Wu, J. Bao, H.T. Wu*, Y.Y. Zhou**

School of Materials Science and Engineering, University of Jinan, Jinan, 250022, China

ARTICLE INFO

Keywords:
$Gd_2Zr_3(MoO_4)_9$
Microwave dielectric properties
Chemical bonds theory of complex crystals
Far infrared spectrum

ABSTRACT

A new $Gd_2Zr_3(MoO_4)_9$ (GZM) ceramic was prepared using the solid-state method at a low sintering temperature. A single phase, with trigonal structure in R-3c space group, was confirmed by the X-ray diffractometer. The crystal structure was further investigated through the Rietveld refinement results. Scanning electron microscopy characterized the dense GZM samples sintered at 725–800 °C with homogeneous microstructures. The chemical bonds theory of complex crystals was employed to investigate the structure-property relations of GZM samples in detail. The intrinsic properties were explored by the far-infrared spectrum, and the calculated microwave dielectric properties were in good agreement with the measured values. It could be concluded that the microwave dielectric property of GZM was mainly ascribed to the ion polarization rather electronic. The optimum microwave dielectric properties with a permittivity (ε_r) of 10.78, a quality factor ($Q{\cdot}f$) of 40,945 GHz and a temperature coefficient of resonant frequency (τ_f) of −12.26 ppm/°C were achieved in GZM sample sintered at 725 °C.

1. Introduction

The microwave devices with good microwave dielectric performances have been widely investigated due to the explosive growth of high frequency wireless communication technology [1–3]. Materials with high ε_r values for the demands of miniaturization, high $Q{\cdot}f$ values to improve frequency selectivity, near-zero τ_f values for good temperature stabilities and low sintering temperatures to co-fire with electrodes should be indispensably taken into consideration to design the low-temperature co-fired ceramics (LTCC) devices [4]. It is desirable to develop novel microwave dielectric material systems [5–9], improve microwave dielectric properties by ion substitutions [10–12] and lower sintering temperatures by adding sintering additives [13–15]. Up to now, a great number of new dielectric materials with low sintering temperatures have been widely studied, such as $Li_9Zr_3NbO_{13}$ [16], (1-x)$BaCu(B_2O_5)$-xTiO_2 [17], $Ca_{0.66}Bi_{0.34}Mo_{0.66}V_{0.34}O_4$ [18] and $Li_3Ba_2La_{1.8}Y_{1.2}(MoO_4)_8$ [19] ceramics, and they might be promising candidates for LTCC applications.

Recently, due to the low sintering temperatures and excellent microwave dielectric properties, Mo-based microwave dielectric ceramics such as $Sm_2Zr_3(MoO_4)_9$, $Nd_2Zr_3(MoO_4)_9$ and $Eu_2Zr_3(MoO_4)_9$ have achieved great attention [20–23]. For example, good microwave dielectric properties of ε_r = 10.8, $Q{\cdot}f$ = 50,628 GHz and τ_f = −38.8 ppm/°C were achieved in $La_2Zr_3(MoO_4)_9$ sample [22]. Subsequently, in order to improve the dielectric properties, $La_2(Zr_{0.92}Ti_{0.08})_3(MoO_4)_9$ sample sintered at 750 °C with excellent microwave dielectric properties of ε_r = 10.33, $Q{\cdot}f$ = 80,658 GHz and τ_f = 3.48 ppm/°C was prepared [23]. However, a new $Gd_2Zr_3(MoO_4)_9$ ceramic has not been reported before. Therefore, a new GZM ceramic was prepared successfully by the solid-state route for the first time. The microstructures, sintering characteristics and dielectric properties of GZM were studied scientifically. The chemical bonds theory of complex crystals and infrared (IR) reflectivity spectrum were used to explore the relationships between the intrinsic factors and microwave dielectric properties of GZM samples.

2. Experimental procedure

$Gd_2Zr_3(MoO_4)_9$ composition was prepared using the solid-state method with reagent-grade powders of Gd_2O_3 (99.9%, Macklin, China), ZrO_2 (99.99%, Macklin, China) and MoO_3 (99.9%, Macklin, China). The stoichiometric mixtures were milled with ethanol and zirconia balls for 24 h. The resulting slurry was dried after milling. After calcination at 750 °C for 2 h, the powders were re-milled again for 24 h. After drying,

* Corresponding author.
** Corresponding author.
E-mail addresses: mse_wuht@ujn.edu.cn (H.T. Wu), mse_zhouyy@ujn.edu.cn (Y.Y. Zhou).

https://doi.org/10.1016/j.ceramint.2019.07.243
Received 20 June 2019; Received in revised form 15 July 2019; Accepted 20 July 2019

the powders that added with 10% PVA as a binder were pressed into pellets (10 mm in diameter and 6 mm in height) under an axial pressure of 200 MPa. Subsequently, the PVA binder additions of samples were expelled. At last, the GZM ceramics were sintered at 675–800 °C for 6 h in air.

The XRD (Brucker D8) was used to analyse crystal structures of GZM. The microstructures of sintered samples were observed by SEM (FeSEM Quanta 250, FEI Co., USA). IR reflectivity spectrum was analysed via a Bruker IFS 66v FT-IR spectrometer. The network analyzer (N5234A, Agilent Co., USA) was used to measure the ε_r and $Q{\cdot}f$ values [24,25]. The τ_f value was obtained using the equation:

$$\tau_f = \frac{f_1 - f_0}{f_0 \times \Delta T} \times 10^6 (ppm/°C) \quad (1)$$

where f_0 and f_1 were the resonant frequency at 25 °C and 85 °C, respectively. The apparent densities were measured via the Archimedes method. The theoretical densities can be obtained through Eq. (2):

$$\rho_{theory} = \frac{ZA}{V_c N_A} \quad (2)$$

where A and Z are the atomic weight (g/mol) and number of atoms in unit cell, respectively; N_A is Avogadro number (mol^{-1}), and V_c is volume of unit cell (cm^3). The following formula is used to calculate the relative density:

$$\rho_{relative} = \frac{\rho_{apparent}}{\rho_{theory}} \times 100\,\% \quad (3)$$

3. Results and discussion

The X-ray diffraction patterns of calcined powders sintered at 750 °C and GZM samples sintered at 675–800 °C were carried out in Fig. 1. All the diffraction peaks corresponded to pure trigonal GZM (JCPDS # 54-0052) without any secondary phases, which indicated that a solid solution of the GZM phase was formed in the temperature range of 675–800 °C. To further investigate the structure variations of GZM samples sintered at 675–800 °C, Rietveld refinements (shown in Fig. 2) were employed, and the refinement results were exhibited in Table 1. R_p, R_{wp} and χ^2 values were found to be in the range of 5.14–5.65, 6.97–7.53 and 1.39–1.65, respectively. The low residual factors (R_{wp}, R_p) confirmed the phase purity of GZM. In addition, the lattice parameters of $a = b$, c and V were measured as 9.7750–9.7762 Å, 57.9459–57.9669 Å and 4795.03–4797.74 $Å^3$, respectively. The schematic crystal structure of GZM was presented in Fig. 3, in which Gd, Zr (1), Zr(2), Mo(1), Mo(2) and O atoms had 9, 6, 6, 4, 4 and 2 nearest oxygen neighbours occupying the Wyckoff sites of 12c, 6b, 12c, 36f, 18e and 36f, respectively. In addition, it could be seen that all polyhedrons were connected by shared oxygen atoms at the vertices.

Fig. 4 reveled the variation tendencies of the apparent and relative densities of GZM samples sintered at 675–800 °C for 6 h. With temperature increasing, apparent density increased from 3.66 g/cm^3 at 675 °C to 3.85 g/cm^3 at 725 °C, then saturated at 725–800 °C. The relative density of GZM possessed the same trend as apparent density, and the saturated value of 92.12% was achieved at 725–800 °C. Typical SEM images of fractured surfaces of GZM samples sintered at 675–800 °C were illustrated in Fig. 5. When the sintering temperature increased from 675 to 725 °C, the pores gradually disappeared. It was seen that GZM could be well sintered at 725–800 °C, which was consistent with the result of density.

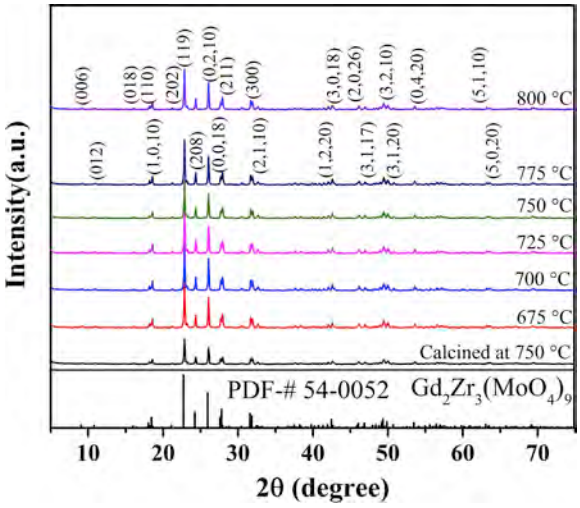

Fig. 1. X-Ray diffraction patterns of calcined powders sintered at 750 °C for 2 h and $Gd_2Zr_3(MoO_4)_9$ ceramics sintered at 675–800 °C for 6 h.

Fig. 6 showed the microwave dielectric properties of the GZM samples sintered at different temperatures. The permittivity ε_r increased linearly from 7.75 at 675 °C to the maximum value of 13.60 at 725 °C due to the elimination of pores before reaching a stable state. The variation in permittivity versus sintering temperature presented similar behavior to that of density, suggesting that density acted as a main influencing factor of permittivity, where higher ε_r value was obtained correspondingly with higher density as shown in Fig. 4. The $Q{\cdot}f$ value of GZM sample first increased from 6370 GHz at 675 °C to 42,754 GHz at 700 °C, and kept stable at 41,201 GHz in the temperature range of 700–750 °C. With further increasing firing temperature, $Q{\cdot}f$ decreased slightly, which might be caused by over-sintering. In addition, with an increase in temperature from 675 to 800 °C, the saturation τ_f value of −10.69 ppm/°C was obtained. Therefore, a novel temperature-stable GZM ceramic sintered at 725 °C with optimum dielectric properties of ε_r = 10.78, $Q{\cdot}f$ = 40,945 GHz and τ_f = −12.26 ppm/°C was obtained.

In general, the microwave dielectric properties are associate with the extrinsic factors, including density, the secondary phase, grain size, impurities, pores, etc., and intrinsic factors, dependent on the structure characteristics [23]. The extrinsic factors almost can be neglected in optimum ceramics because of the homogeneous and dense microstructures and no secondary phases. The chemical bond parameters (bond ionicity f_i, lattice energy U, bond energy E, coefficient of thermal expansion α) of complex crystals were obtained to investigate the influences of chemical bonds on crystal structures, and then the relationships between bond characteristics and microwave dielectric properties of GZM samples were also discussed in detail.

Based on the Phillips-Van Vechten-Levine (P–V-L) theory, the sum of binary crystals could be written as shown in Eq. (4) [26–28]. Effective valence of Gd, Zr and Mo were P_{Gd} = 3, P_{Zr} = 4 and P_{Mo} = 6, respectively. The effective valence of O should be followed by the subformula. The effective valence electron numbers of cations were Z_{Gd} = 3, Z_{Zr} = 4 and Z_{Mo} = 6, while the effective valence electron numbers of anions were Z_O = 2 in Gd–O bond, Z_O = 4 in Zr–O bond and Z_O = 9 in Mo–O bond. Therefor, the effective valence electron numbers of Gd–O bond, Zr–O bond and Mo–O bond were 4/3, 8/3 and 6, respectively.

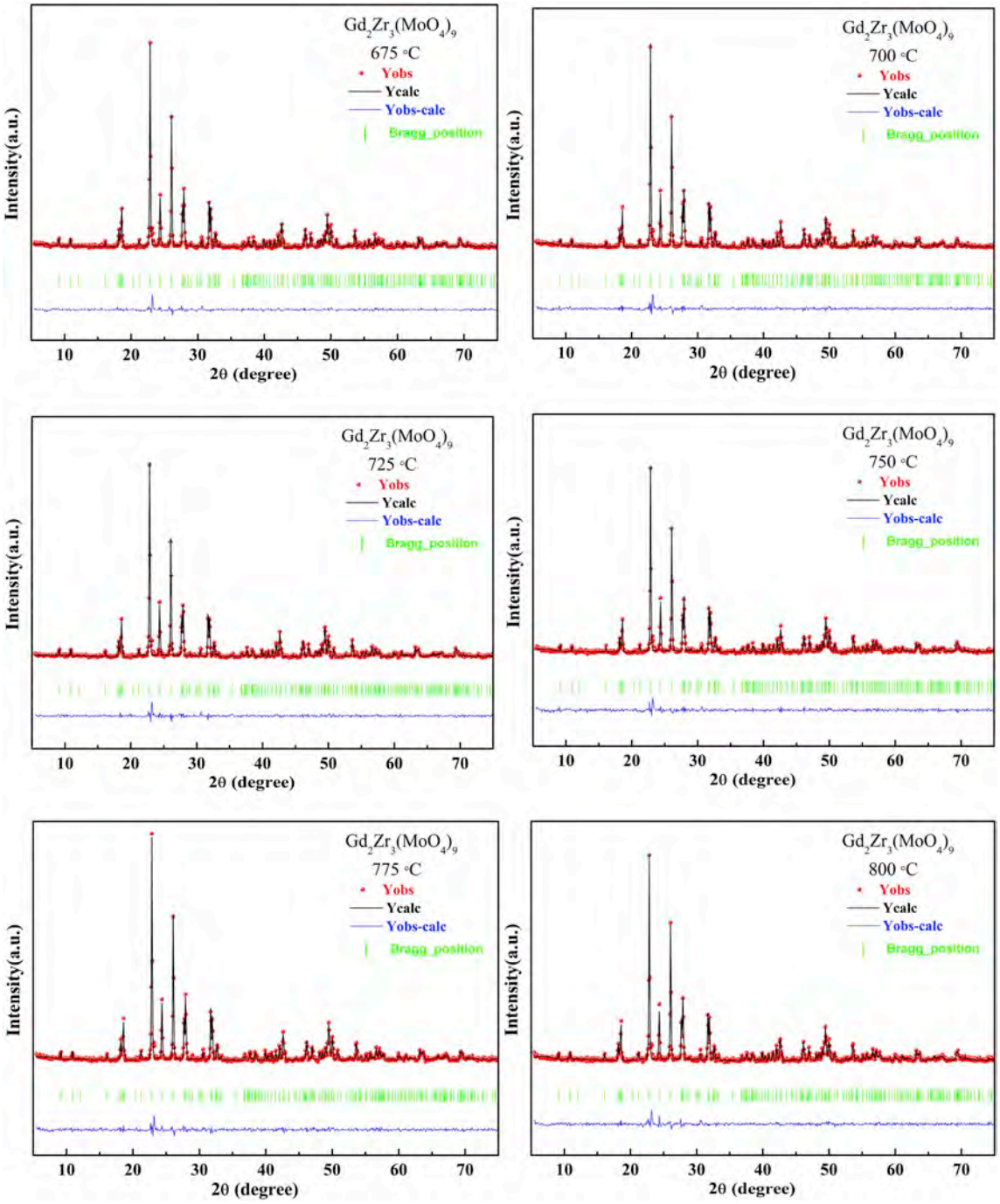

Fig. 2. Rietveld refinements of $Gd_2Zr_3(MoO_4)_9$ ceramics sintered at 675–800 °C for 6 h.

$$\begin{aligned} Gd_2Zr_3(MoO_4)_9 \rightarrow\ & Gd_2 + Zr(1) + Zr(2)_2 + Mo(1)_6 + Mo(2)_3 \\ & + O(1)_6 + O(2)_6 + O(3)_6 + O(4)_6 + O(5)_6 + O(6)_6 \\ & \rightarrow Gd_{2/3}O(1)_3 + Gd_{2/3}O(2)_3 + Gd_{2/3}O(6)_3 \\ & + Zr(1)O(4)_3 + Zr(2)O(3)_3 + Zr(2)O(5)_3 \\ & + Mo(1)_{3/2}O(1)_3 + Mo(1)_{3/2}O(2)_3 + Mo(1)_{3/2}O(3)_3 \\ & + Mo(1)_{3/2}O(4)_3 + Mo(2)_{3/2}O(5)_3 + Mo(2)_{3/2}O(6)_3 \end{aligned} \quad (4)$$

Based on Eq. (5), the permittivity can be predicted using bond ionicity [29], and the f_i value of any μ bond can be expressed as Eqs. (6)–(9) [26–28]:

$$\varepsilon = \frac{n^2 - 1}{1 - f_i} + 1 \quad (5)$$

Table 1
The lattice parameters, theoretical densities and reliability factors of $Gd_2Zr_3(MoO4)_9$ ceramics sintered at 675–800 °C for 6 h.

S.T. (°C)	$a=b$ (Å)	c (Å)	$\alpha=\beta$ (°)	γ (°)	V (Å^3)	R_p (%)	R_{wp} (%)	χ^2	$\rho_{theo.}$ (g/cm^3)
675	9.776(2)	57.949(7)	90	120	4796.44	5.36	7.40	1.63	4.213(2)
700	9.775(1)	57.945(9)	90	120	4795.03	5.45	7.37	1.65	4.214(5)
725	9.775(0)	57.951(9)	90	120	4795.51	5.14	6.97	1.57	4.214(0)
750	9.775(9)	57.954(1)	90	120	4796.49	5.42	7.18	1.39	4.213(2)
775	9.775(8)	57.961(7)	90	120	4797.03	5.43	7.21	1.50	4.212(7)
800	9.776(0)	57.966(9)	90	120	4797.74	5.65	7.53	1.57	4.212(1)

S.T.— the sintering temperature of $Gd_2Zr_3(MoO_4)_9$ ceramics.
$\rho_{theo.}$— theoretical density of $Gd_2Zr_3(MoO_4)_9$ ceramics.
R_p— reliability factor of patterns.
R_{wp}— reliability factor of weighted pattern.
χ^2— goodness of fit indicator.

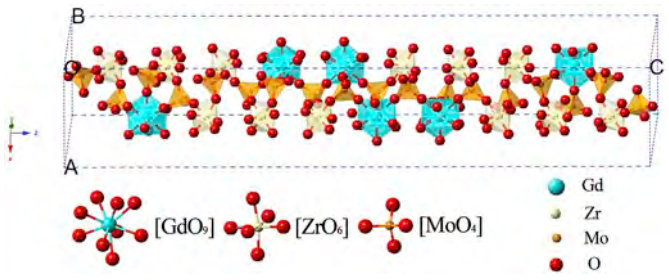

Fig. 3. Schematic representation of the crystal structure for $Gd_2Zr_3(MoO_4)_9$ ceramic.

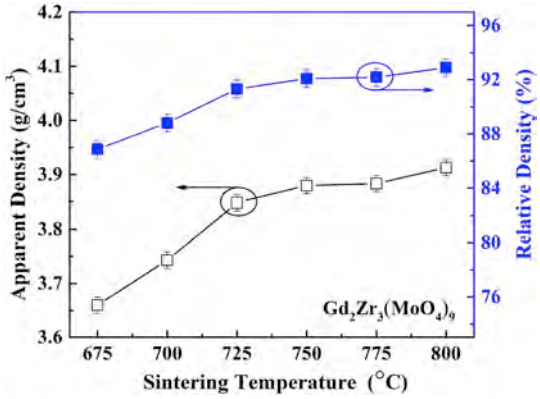

Fig. 4. Apparent densities and relative densities of $Gd_2Zr_3(MoO_4)_9$ ceramics sintered at 675–800 °C for 6 h.

$$f_i^{\mu} = \frac{(C^{\mu})^2}{(E_g^{\mu})^2} \tag{6}$$

$$(E_g^{\mu})^2 = (E_h^{\mu})^2 + (C^{\mu})^2 \tag{7}$$

$$(E_h^{\mu})^2 = \frac{39.74}{(d^{\mu})^{2.48}} \tag{8}$$

$$C^{\mu} = 14.4b^{\mu}\exp(-k_s^{\mu}r_0^{\mu})\left[(Z_A^{\mu})^* - \frac{n}{m}(Z_B^{\mu})^*\right]/r_0^{\mu} \tag{9}$$

where the average energy gap E_g^{μ} is decomposed to the homopolar part E_h^{μ} and heteropolar part C^{μ}, and $\exp(-k_s^{\mu}r_0^{\mu})$ is thomas-Fermi screening factor [30]. The calculated results were displayed in Table 2, and Fig. 7(a) showed the average bond ionicity of any μ bond. The largest f_i value of 85.03% was achieved in Gd–O bond, suggesting that the f_i value of Gd–O bond played a peredominant role in affecting the ε_r value of GZM sample. In addition, the polarizability is also help to investigate the influence of intrinsic factor on permittivity.

$$\begin{aligned}\alpha_{theo.} &= \alpha(Gd_2Zr_3(MoO_4)_9)\\ &= 2\alpha(Gd^{3+}) + 3\alpha(Zr^{4+}) + 9\alpha(Mo^{6+}) + 36\alpha(O^{2-})\end{aligned} \tag{10}$$

$$\alpha_{obs.} = \frac{1}{b}V_m\frac{\varepsilon_r - 1}{\varepsilon_r + 2} \tag{11}$$

where $\alpha(Gd^{3+})$, $\alpha(Zr^{4+})$ and $\alpha(O^{2-})$ are the theoretical ion polarizabilities reported by Shannon et al. [31], $\alpha(Mo^{6+})$ is calculated by Choi et al. [32], b is a constant value ($4\pi/3$), and V_m is the molar volume. The theoretical dielectric polarizability was about 120.37, which was closed to the observed value (146.02), meaning the accuracy of the theoretical calculation of the dielectric polarizability.

Lattice energy U characterizes the binding ability between cations and anions. A crystal structure with high binding energy suggests high stability of crystal structure, that is to say, low intrinsic loss [33]. Therefore, lattice energy can be used to predict the quality factor of microwave dielectric ceramics, which is decomposed into ionic part U_{bi}^{μ} and covalent part U_{bc}^{μ}. The lattice energy of GZM sample was evaluated by Eq. (12)-(15) [26–28]:

$$U_{cal} = \sum_{\mu} U_b^{\mu} \tag{12}$$

$$U_b^{\mu} = U_{bc}^{\mu} + U_{bi}^{\mu} \tag{13}$$

$$U_{bc}^{\mu} = 2100m\frac{(Z_A^{\mu})^{1.64}}{(d^{\mu})^{0.75}}f_C^{\mu} \tag{14}$$

$$U_{bi}^{\mu} = 1270\frac{(m+n)Z_A^{\mu}Z_B^{\mu}}{d^{\mu}}\left(1 - \frac{0.4}{d^{\mu}}\right)f_i^{\mu} \tag{15}$$

After calculation, the average lattice energies of Gd–O, Zr–O and

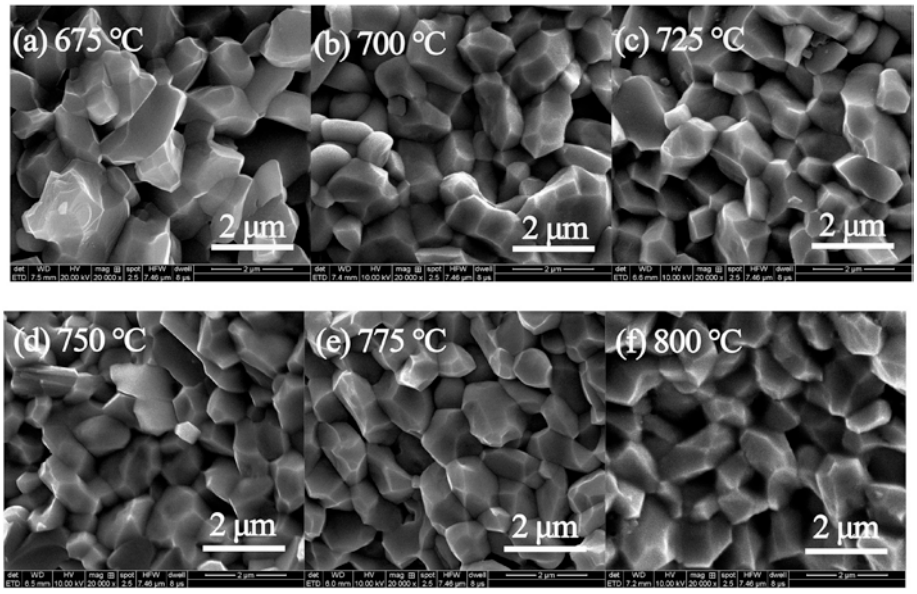

Fig. 5. SEM micrographs of fractured surfaces of $Gd_2Zr_3(MoO_4)_9$ ceramics sintered at different temperatures for 6 h (a-e corresponding to 675–800 °C).

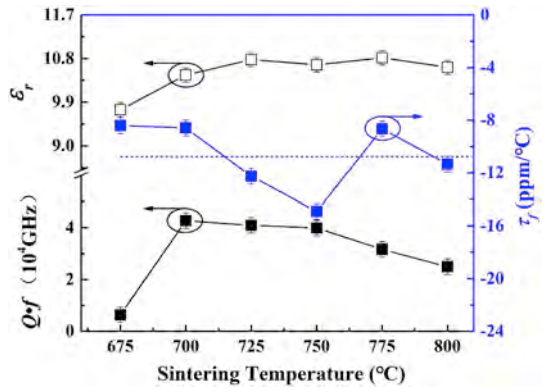

Fig. 6. The microwave dielectric properties of $Gd_2Zr_3(MoO_4)_9$ ceramics sintered at 675–800 °C for 6 h.

Mo–O bonds were 3335.89, 10988.00 and 43180.38 kJ/mol, respectively. According to Fig. 7(b) and Table 2, the sequence of U (Mo–O) > U (Zr–O) > U (Gd–O) suggested that Mo–O bond provided the majority contributions to quality factors of GZM ceramics.

Moreover, E is a performance index to measure the strength of chemical bonds, and the bond energy is calculated based on the following formulas [34–36]:

$$E^{\mu} = t_c E_c^{\mu} + t_i E_i^{\mu} \tag{16}$$

$$t_i = \left| \frac{(S_A - S_B)}{6} \right| \tag{17}$$

$$E_c^{\mu} = \frac{(r_{cA} + r_{cB})}{d^{\mu}} (E_{A-A} E_{B-B})^{1/2} (KJ/mol) \tag{18}$$

$$E_i^{\mu} = \frac{1389.088}{d^{\mu}} (KJ/mol) \tag{19}$$

$$t_c + t_i = 1 \tag{20}$$

where S_A and S_B are the electronegativities of A and B ions; r_{cA} and r_{cB} are the covalent radii; t_i and t_c are ionic and covalent proportional coefficient of an individual bond μ; homonucler bond energy $E_{A\text{-}A}$ and $E_{B\text{-}B}$ can be consulted in handbook of bond energies [37]. Based on the calculated result (E (Mo–O) > E (Zr–O) > E (Gd–O)) of Table 2 and Fig. 7(c), it might be concluded that Mo–O bond provided a major contribution to GZM structure.

The correlation among the temperature coefficient of resonant frequency τ_f, temperature coefficient of the dielectric constant τ_ε and coefficient of thermal expansion α is shown in Eq. (21), in which α is calculated from Eq. 22–25:

$$\tau_f = -(\frac{\tau_\varepsilon}{2} + \alpha) \tag{21}$$

$$\alpha = \sum_{\mu} F_{mn}^{\mu} \alpha_{mn}^{\mu} \tag{22}$$

$$\alpha_{mn}^{\mu} = -3.1685 + 0.8376\gamma_{mn} \tag{23}$$

$$\gamma_{mn} = \frac{k Z_A^{\mu} N_{CA}^{\mu}}{U_b^{\mu} \Delta_A} \beta_{mn} \tag{24}$$

$$\beta_{mn} = \frac{m(m+n)}{2n} \tag{25}$$

where F_{mn}^{μ} is the proportion of μ bond, N_{CA}^{μ} is the coordination number of μ bond for cation, Z_A^{μ} is the valence states of cation, and k is Boltzmann constant. The temperature coefficient of resonant frequency is inversely proportional to the coefficient of thermal expansion. The average α of Gd–O, Zr–O and Mo–O were 10.0204×10^{-6}/K, 3.3368×10^{-6}/K and -0.3765×10^{-6}/K, respectively. Therefore, the α values of Gd–O and Zr–O bonds ($\alpha_{Gd\text{-}O,\ Zr-O} > 0$) had a negative effect on the temperature coefficients of resonant frequency, and the main

Table 2
Bond ionicity f_i, lattice energy U, bond energy E and the coefficient of thermal expansion α of each bond for $Gd_2Zr_3(MoO_4)_9$ ceramic sintered at 725 °C for 6 h.

Bond type	d (Å)	f_i^μ	f_c^μ	E_i (kJ/mol)	E_c (kJ/mol)	E (kJ/mol)	U_{bc} (kJ/mol)	U_{bi} (kJ/mol)	U (kJ/mol)	α ($10^{-6}K^{-1}$)
Gd–O(1)[1]	2.481(4)	0.851(1)	0.148(9)	559.532(5)	299.786(7)	396.325(6)	639	2680	3319	10.085(5)
Gd–O(1)[2]	2.482(0)	0.851(2)	0.148(8)	559.397(3)	299.714(3)	396.229(8)	639	2679	3318	10.089(5)
Gd–O(1)[3]	2.482(4)	0.851(2)	0.148(8)	559.307(1)	299.666(0)	396.165(9)	638	2679	3317	10.093(5)
Gd–O(2)[1]	2.417(3)	0.847(5)	0.152(5)	574.369(8)	307.736(2)	406.835(0)	667	2725	3392	9.800(3)
Gd–O(2)[2]	2.417(5)	0.847(5)	0.152(5)	574.322(2)	307.710(8)	406.801(4)	667	2725	3392	9.800(3)
Gd–O(2)[3]	2.417(9)	0.847(6)	0.152(4)	574.227(2)	307.659(9)	406.734(1)	667	2725	3392	9.800(3)
Gd–O(6)[1]	2.499(4)	0.852(1)	0.147(9)	555.502(9)	297.627(8)	393.471(4)	631	2667	3298	10.169(9)
Gd–O(6)[2]	2.499(6)	0.852(1)	0.147(9)	555.458(5)	297.603(9)	393.439(9)	631	2667	3298	10.169(9)
Gd–O(6)[3]	2.500(1)	0.852(1)	0.147(9)	555.3474)	297.5444)	393.3612)	631	2666	3297	10.174(0)
Zr(1)–O(4) × 6	2.026(0)	0.788(6)	0.211(4)	685.303(1)	412.900(8)	508.695(6)	2539	8464	11003	3.317(8)
Zr(2)–O(3)[1]	2.187(7)	0.801(1)	0.198(9)	634.650(1)	382.381(9)	471.096(2)	2255	8108	10363	3.718(4)
Zr(2)–O(3)[2]	2.188(3)	0.801(2)	0.198(8)	634.476(1)	382.277(1)	470.967(1)	2254	8106	10360	3.720(4)
Zr(2)–O(3)[3]	2.188(4)	0.801(2)	0.198(8)	634.447(1)	382.259(6)	470.945(6)	2254	8106	10360	3.720(4)
Zr(2)–O(5)[1]	1.893(8)	0.776(3)	0.223(7)	733.141(8)	441.724(0)	544.206(0)	2826	8761	11587	2.990(9)
Zr(2)–O(5)[2]	1.894(2)	0.776(4)	0.223(6)	732.987(0)	441.630(8)	544.091(0)	2825	8760	11585	2.991(9)
Zr(2)–O(5)[3]	1.894(7)	0.776(4)	0.223(6)	732.793(6)	441.514(2)	543.947(5)	2824	8759	11583	2.993(0)
Mo(1)–O(1)	1.682(1)	0.719(2)	0.280(8)	825.411(1)	556.685(5)	614.013(6)	11312	33522	44834	−0.482(3)
Mo(1)–O(2)	1.808(5)	0.732(4)	0.267(6)	767.721(3)	517.777(5)	571.098(9)	10209	32445	42654	−0.345(0)
Mo(1)–O(3)	1.730(9)	0.724(6)	0.275(4)	802.139(9)	540.990(6)	596.702(5)	10859	33110	43969	−0.429(4)
Mo(1)–O(4)	1.870(1)	0.738(0)	0.262(0)	742.433(0)	500.722(3)	552.287(2)	9746	31914	41660	−0.277(6)
Mo(2)–O(5) × 2	1.876(8)	0.738(6)	0.261(4)	739.782(6)	498.934(7)	550.315(6)	9699	31856	41555	−0.270(3)
Mo(2)–O(6) × 2	1.694(7)	0.720(6)	0.279(4)	819.274(2)	552.546(6)	609.448(5)	11192	33416	44608	−0.468(7)
Gd-$O_{avg.}$	2.466(4)	0.850(3)	0.149(7)	–	–	398.818(2)	–	–	3336	10.020(4)
Zr-$O_{avg.}$	2.033(6)	0.788(7)	0.211(3)	–	–	508.118(9)	–	–	10988	3.336(8)
Mo-$O_{avg.}$	1.779(3)	0.729(1)	0.270(9)	–	–	581.703(8)	–	–	43180	−0.376(5)

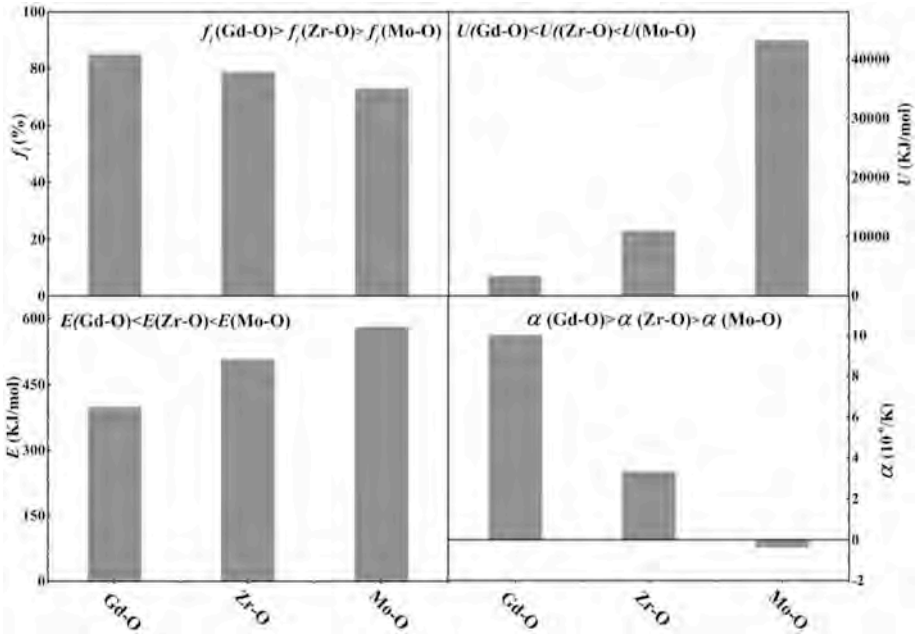

Fig. 7. (a) Bond ionicity f_i; (b) lattice energy U; (c) bond energy E; and (d) the coefficient of thermal expansion α for $Gd_2Zr_3(MoO_4)_9$ ceramic sintered at 725 °C for 6 h.

positive effect to temperature coefficients of resonant frequency was the α values of Mo–O bond ($\alpha_{Mo\text{-}O} < 0$).

The IR reflectivity spectrum of GZM sintered at 725 °C was collected within the range of 50–1500 cm^{-1} (Fig. 8(a)), which was also a useful tool to analyse the intrinsic dielectric properties of the sintered samples. The reflectivity spectrum was fitted by using the classical harmonic oscillator model, and the fitted spectrum conformed well with the measured spectrum as shown in Fig. 8(a). Based on the space group theory, the vibrational representations of GZM with a space group of R-3c (No. 167) and a point group of D_{3d} (-3m) were shown in Table 3 [38]. The classifications of IR vibrational modes were shown in Table 4 [39]. According to the theoretical prediction, there are 75 infrared

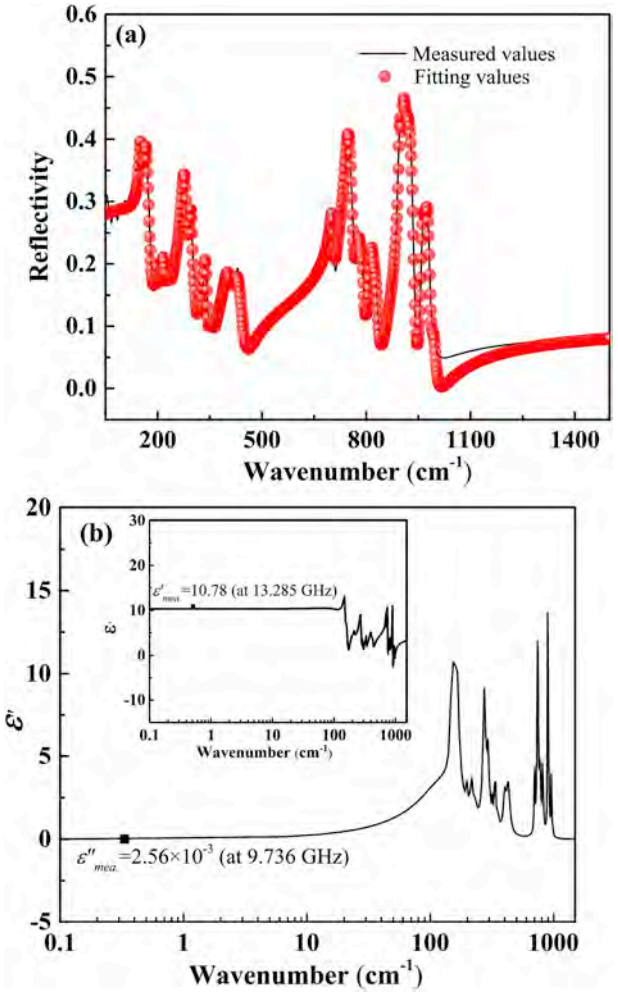

Fig. 8. (a) Measured (black line) and fitted (red line) IR reflectivity spectrum of $Gd_2Zr_3(MoO_4)_9$ ceramic sintered at 725 °C for 6 h; (b) Real and imaginary parts of complex permittivity for $Gd_2Zr_3(MoO_4)_9$ ceramic sintered at 725 °C for 6 h (points are measured values at microwave region). (For interpretation of the references to colour in this figure legend, the reader is referred to the Web version of this article.)

Table 3
Character table of irreducible representations.

D_{3d} (-3m)	E	$2C_3$	$3C_2$	i	$2S_6$	$3\sigma_d$	selection rule
$A_{1g}\Gamma_1^+$	1	1	1	1	1	1	$\sigma_{xx}+\sigma_{yy}$, σ_{zz}
$A_{2g}\Gamma_2^+$	1	1	−1	1	1	−1	R_z
$E_g\Gamma_3^+$	2	−1	0	2	−1	0	(R_x, R_y), (σ_{xx}-σ_{yy}, σ_{xy}), (σ_{xz}, σ_{yz})
$A_{1u}\Gamma_1^-$	1	1	1	−1	−1	−1	–
$A_{2u}\Gamma_2^-$	1	1	−1	−1	−1	1	T_z
$E_u\Gamma_3^-$	2	−1	0	−2	1	0	(T_x, T_y)

vibrational modes, which can be expressed as $\Gamma_{IR} = 25A_{2u}+50E_u$ (acoustic modes not included). As the representations show, each atom at a designated position exhibits a unique vibration. For instance, the corresponding infrared active modes of Gd and Zr(2) atoms at the 12c Wyckoff position are $A_{2u}+2E_u$. However, the experimental amounts of IR active modes were 26 as shown in Table 5, which might be caused by the overlay and degeneracy of the modes.

The complex dielectric permittivity $\varepsilon^*(\omega)$ is calculated as shown in Eq. (26), and the complex reflectivity R can be obtained as Eq. (27) [40]:

$$\varepsilon^*(\omega) = \varepsilon_\infty + \sum_{j=1}^{n} \frac{\omega_{pj}^2}{\omega_{oj}^2 - \omega^2 + j\omega\gamma_j} \tag{26}$$

$$R = \left| \frac{1-\sqrt{\varepsilon^*(\omega)}}{1+\sqrt{\varepsilon^*(\omega)}} \right|^2 \tag{27}$$

where the optical permittivity ε_∞ is only produced by the electronic polarization; ω_{oj}, ω_{pj} and γ_j are the eigen frequency, plasma frequency and damping factor, respectively; n is the number of transverse phonon modes. In addition, the following formula is used to calculate the dielectric loss tangent tan δ:

$$\tan\delta = \frac{\varepsilon''}{\varepsilon'} = \frac{\sum_{j=1}^{n} \Delta\varepsilon_j(\gamma_j\omega)/\omega_{oj}^2}{\varepsilon_\infty + \sum_{j=1}^{n}\Delta\varepsilon_j} \tag{28}$$

Fig. 8(b) showed the fitted infrared reflectivity values and complex permittivities. The extra-polated permittivity of GZM was 10.33, which was close to the measured value (10.78). The calculated dielectric loss and the experimental value had the same order of magnitudes. In addition, the optical permittivity from the IR spectrum of the GZM is 3.72, which was 36.01% of the total polarizability contribution at microwave frequencies, suggesting that the main polarization contributions to ε_r came from ionic polarization rather than electronic.

4. Conclusion

A novel trigonal-type GZM ceramics with low sintering temperatures were prepared for the first time, and pure phase was synthesized in the whole temperature range of 675–800 °C. Rietveld refinement parameters of $a = b$ = 9.7750–9.7762 Å, c = 57.9459–57.9669 Å and V = 4795.03–4797.74 Å^3 could be obtained. SEM showed that dense and homogeneous grains could be formed when the samples sintered at 725–800 °C. The chemical bond parameters of GZM sample sintered at 725 °C were obtained to explore the relationships between intrinsic factors and dielectric properties, and the variations of ε_r, $Q{\cdot}f$ and τ_f values could be mainly caused by the Gd/Mo–O bond parameters. Infrared reflectivity spectrum analysis exhibited that the main contribution to microwave dielectric property was ion polarization. Typically, GZM sample sintered at 725 °C exhibited optimum microwave dielectric properties of ε_r = 10.78, $Q{\cdot}f$ = 40,945 GHz and τ_f = −12.26 ppm/°C.

Table 4
IR vibrational modes of the $Gd_2Zr_3(MoO_4)_9$ structure.

atom	Position	Symmetry	Irreducible Vibrational Representations	IR Active Modes
Gd, Zr(2)	12c	C_3	$A_{1g}+A_{1u}+A_{2g}+A_{2u}+2E_u+2E_g$	$A_{2u}+2E_u$
Zr(1)	6b	S_6	$A_{1u}+A_{2u}+2E_u$	$A_{2u}+2E_u$
Mo(1), O(1), O(2), O(3), O(4), O(5), O(6)	36f	C_1	$3A_{1g}+3A_{1u}+3A_{2g}+3A_{2u}+6E_u+6E_g$	$3A_{2u}+6E_u$
Mo(2)	18e	C_2	$A_{1g}+A_{1u}+2A_{2g}+2A_{2u}+3E_u+3E_g$	$2A_{2u}+3E_u$

$\Gamma_{optic} = 24A_{1g}+25A_{1u}+25A_{2g}+25A_{2u}+50E_u+49E_g$.
$\Gamma_{acoustic} = A_{2u}+E_u$.
$\Gamma_{IR} = 25A_{2u}+50E_u$ (Acoustic modes not included).
$\Gamma_{Raman} = 24A_{1g}+49E_g$.

Table 5
Phonon parameters obtained from the fitting of the infrared spectrum $Gd_2Zr_3(MoO_4)_9$ ceramic sintered at 725 °C for 6 h.

Mode	ε_∞ = 3.72			
	ω_{oj}	ω_{pj}	γ_j	$\Delta\varepsilon_j$
1	143.94	253.58	144.28	3.100
2	151.12	92.96	8.62	0.378
3	164.24	146.35	16.63	0.794
4	198.99	35.09	5.64	0.031
5	217.35	72.34	12.49	0.111
6	232.79	49.49	13.91	0.045
7	275.42	192.72	16.92	0.490
8	293.86	115.49	11.75	0.154
9	305.84	73.65	17.39	0.058
10	320.53	49.75	6.62	0.024
11	336.87	111.89	11.50	0.110
12	355.48	63.50	16.25	0.032
13	402.43	133.59	22.77	0.110
14	429.82	211.32	35.12	0.242
15	702.73	174.92	10.43	0.062
16	745.29	426.30	20.83	0.327
17	777.93	237.28	21.54	0.093
18	788.44	77.37	9.47	0.010
19	814.52	155.80	12.23	0.037
20	823.73	218.50	26.20	0.070
21	896.10	245.58	6.76	0.075
22	903.70	297.21	12.79	0.108
23	915.21	259.89	25.52	0.081
24	960.42	200.76	12.81	0.044
25	970.90	116.18	14.69	0.014
26	992.23	78.79	16.11	0.006

ω_{oj}, ω_{pj} and γ_j are the the eigen frequency, plasma frequency, damping factor and calculated ε of individual mode, ε_∞ is the dielectric constant affected by electronic polarization in higher frequencies.

Acknowledgments

This work was supported by the National Natural Science Foundation of China (No. 51472108 and 51872119). The authors are thankful to the help of Professor ZhenXing Yue and postdoctoral Jie Zhang on the measurement of microwave properties in Tsinghua University. The authors are also thankful to the administrators in IR beamline workstation of National Synchrotron Radiation Laboratory for the help in IR measurement.

References

[1] D. Zhou, L.X. Pang, D.W. Wang, C. Li, B.B. Jin, I.M. Reaney, High permittivity and low loss microwave dielectrics suitable for 5G resonators and low temperature co-fired ceramic architecture, J. Mater. Chem. C 5 (2017) 10094–10098.
[2] L.X. Pang, D. Zhou, Modification of $NdNbO_4$ microwave dielectric ceramic by Bi substitutions, J. Am. Ceram. Soc. 102 (2019) 2278–2282.
[3] X.K. Lan, J. Li, Z.Y. Zou, G.F. Fan, W.Z. Lu, W. Lei, Lattice structure analysis and optimised microwave dielectric properties of $LiAl_{1-x}(Zn_{0.5}Si_{0.5})_xO_2$ solid solutions, J. Eur. Ceram. Soc. 39 (2019) 2360–2364.
[4] S.Z. Hao, D. Zhou, L.X. Pang, The spectra analysis and microwave dielectric properties of $[Ca_{0.55}(Sm_{1-x}Bi_x)_{0.3}]MoO_4$ ceramics, J. Am. Ceram. Soc. 102 (2019) 3103–3109.
[5] D. Zhou, L.X. Pang, D.W. Wang, I.M. Reaney, Novel water-assisting low firing MoO_3 microwave dielectric ceramics, J. Eur. Ceram. Soc. 39 (2019) 2374–2378.
[6] Y. Wang, T.L. Tang, J.T. Zhang, W.S. Xia, L.W. Shi, Preparation and microwave dielectric properties of new low-loss $NiZrTa_2O_8$ ceramics, J. Alloy. Comp. 778 (2019) 576–578.
[7] W.S. Xia, F.Y. Yang, G.Y. Zhang, K. Han, D.C. Guo, New low-dielectric-loss $NiZrNb_2O_8$ ceramics for microwave application, J. Alloy. Comp. 656 (2016) 470–475.
[8] X.Q. Song, K. Du, J. Li, R. Muhammad, W.Z. Lu, X.C. Wang, W. Lei, Crystal structures and microwave dielectric properties of novel low permittivity $Ba_{1-x}Sr_xZnSi_3O_8$ ceramics, Mater. Res. Bull. 112 (2019) 178–181.
[9] Y. Wang, S.B. Zhang, T.L. Tang, W.S. Xia, L.W. Shi, Investigation on microwave dielectric properties of new low-loss $CoZrTa_2O_8$ ceramics, Mater. Lett. 231 (2018) 1–4.
[10] K. Du, X.Q. Song, J. Li, J.M. Wu, W.Z. Lu, X.C. Wang, W. Lei, Optimised phase compositions and improved microwave dielectric properties based on calcium tin silicates, J. Eur. Ceram. Soc. 39 (2019) 340–345.
[11] X.Q. Song, W.Z. Lu, X.C. Wang, X.H. Wang, G.F. Fan, R. Muhammad, W. Lei, Sintering behaviour and microwave dielectric properties of $BaAl_{2-2x}(ZnSi)_xSi_2O_8$ ceramics, J. Eur. Ceram. Soc. 38 (2018) 1529–1534.
[12] W.J. Guo, J. Zhang, Y. Luo, Z.X. Yue, L.T. Li, Microwave dielectric properties and thermally stimulated depolarization of Al-doped $Ba_4(Sm, Nd)_{9.33}Ti_{18}O_{54}$ ceramics, J. Am. Ceram. Soc. 102 (2019) 5494–5502.
[13] W.S. Xia, L.Y. Zhang, Y. Wang, J.T. Zhang, R.R. Feng, L.W. Shi, Optimized sintering properties and temperature stability of $MgZrTa_2O_8$ ceramics with CuO addition for microwave application, J. Mater. Sci. Mater. Electron. 28 (2017) 18437–18441.
[14] Y. Wang, L.Y. Zhang, S.B. Zhang, W.S. Xia, L.W. Shi, Sintering behavior and microwave dielectric properties of $MgZrTa_2O_8$ ceramics with fluoride addition, Mater. Lett. 219 (2018) 233–235.
[15] W.S. Xia, F. Jin, M. Wang, X. Wang, G.Y. Zhang, L.W. Shi, Effects of Al_2O_3 additive on sintering behavior and microwave dielectric properties of $ZnTa_2O_6$ ceramics, J. Mater. Sci. Mater. Electron. 27 (2016) 1100–1104.
[16] H. Yang, B. Tang, Z.X. Fang, J. Luo, S.R. Zhang, A new low-firing and high-Q microwave dielectric ceramic $Li_9Zr_3NbO_{13}$, J. Am. Ceram. Soc. 101 (2018) 2202–2207.
[17] Y.J. Gu, L.W. Lei, J.L. Haung, X.H. Yang, Q. Li, L.H. Li, X.L. Li, B.H. Kim, A novel low-fired, temperature-stable, and low-cost (1-x)$BaCu(B_2O_5)$-xTiO_2 microwave dielectric ceramic, J. Eur. Ceram. Soc. 39 (2019) 1137–1141.
[18] H.H. Guo, D. Zhou, L.X. Pang, Z.M. Qi, Microwave dielectric properties of low firing temperature stable scheelite structured (Ca, Bi)(Mo, V)O_4 solid solution ceramics for LTCC applications, J. Eur. Ceram. Soc. 39 (2019) 2365–2373.
[19] R.Z. Zuo, Y.D. Xu, M. Shi, W.Q. Li, L.G. He, A new series of low-temperature co-firable $Li_3Ba_2La_{3(1-x)}Y_{3x}(MoO_4)_8$ microwave dielectric ceramics, J. Eur. Ceram. Soc. 38 (2018) 4677–4681.
[20] W.Q. Liu, R.Z. Zuo, Low temperature fired $Ln_2Zr_3(MoO_4)_9$ (Ln = Sm, Nd) microwave dielectric ceramics, Ceram. Int. 43 (2017) 17229–17232.
[21] Y.H. Zhang, J.J. Sun, N. Dai, Z.C. Wu, H.T. Wu, C.H. Yang, Crystal structure, infrared spectra and microwave dielectric properties of novel extra low-temperature fired $Eu_2Zr_3(MoO_4)_9$ ceramics, J. Eur. Ceram. Soc. 39 (2019) 1127–1131.
[22] W.Q. Liu, R.Z. Zuo, A novel low-temperature firable $La_2Zr_3(MoO_4)_9$ microwave dielectric ceramic, J. Eur. Ceram. Soc. 38 (2018) 339–342.
[23] Y.H. Zhang, H.T. Wu, Crystal structure and microwave dielectric properties of $La_2(Zr_{1-x}Ti_x)_3(MoO_4)_9$ ($0 \le x \le 0.1$) ceramics, J. Am. Ceram. Soc. 102 (2019) 4092–4102.
[24] B.W. Hakki, P.D. Coleman, A dielectric resonator method of measuring inductive capacities in the millimeter range, IRE Trans. Microw. Theory Tech. 8 (1960) 402–410.
[25] W.E. Courtney, Analysis and evaluation of a method of measuring the complex permittivity and permeability of microwave insulators, IEEE Trans. Microw. Theory Tech. 18 (1970) 476–485.
[26] D.F. Xue, S.Y. Zhang, Calculation of the nonlinear optical coefficient of the $NdAl_3(BO_3)_4$ crystal, J. Phys. Condens. Matter 8 (1996) 1949–1956.
[27] Z.J. Wu, Q.B. Meng, S.Y. Zhang, Semi empirical study on the valences of Cu and bond covalency in $Y_{1-x}Ca_xBa_2Cu_3O_{6+y}$, Phys. Rev. B 58 (1998) 958–962.
[28] Q.B. Meng, Z.J. Wu, S.Y. Zhang, Evaluation of the energy barrier distribution in many-particle systems using the path integral approach, J. Phys. Condens. Matter 10 (1998) 85–88.
[29] S.S. Batsanov, Dielectric methods of studying the chemical bond and the concept of electronegativity, Russ. Chem. Rev. 51 (1982) 684–697.
[30] B.F. Levine, Bond susceptibilities and ionicities in complex crystal structures, J. Chem. Phys. 59 (1973) 1463–1486.
[31] R.D. Shannon, Dielectric polarizabilities of ions in oxides and fluorides, J. Appl. Phys. 73 (1993) 348–366.
[32] G.K. Choi, J.R. Kim, S.H. Yoon, K.S. Hong, Microwave dielectric properties of scheelite (A = Ca, Sr, Ba) and wolframite (A = Mg, Zn, Mn) $AMoO_4$ compounds, J. Eur. Ceram. Soc. 27 (2007) 3063–3067.
[33] H.Y. Yang, S.R. Zhang, Y.W. Chen, H.C. Yang, Y. Yuan, E.Z. Li, Crystal chemistry, Raman spectra, and bond characteristics of trirutile-type $Co_{0.5}Ti_{0.5}TaO_4$ microwave dielectric ceramics, Inorg. Chem. 58 (2019) 968–976.
[34] R.T. Sanderson, Multiple and single bond energies in inorganic molecules, Inorg. Nucl. Chem. Lett. 30 (1968) 375–393.
[35] R.T. Sanderson, Chemical Bonds, Bond Energy, Academic press, New York, 1971.
[36] R.T. Sanderson, Electronegativity and bond energy, J. Am. Chem. Soc. 105 (1983) 2259–2261.
[37] Y.R. Luo, Comprehensive Handbook of Chemical Bond Energies, CRC press, Boca Raton, 2007.
[38] D.L. Rousseau, R.P. Bauman, S.P.S. Porto, Normal mode determination in crystals, J. Raman Spectrosc. 10 (1981) 253–290.
[39] E. Kroumova, M.I. Aroyo, J.M. Perez-Mato, A. Kirov, C. Capillas, S. Ivantchev, H. Wondratschek, Bilbao crystallographic server: useful databases and tools for phase-transition studies, Phase Transitions 76 (2003) 155–170.
[40] D. Zhou, W.B. Li, H.H. Xi, L.X. Pang, G.S. Pang, Phase composition, crystal structure, infrared reflectivity and microwave dielectric properties of temperature stable composite ceramics (scheelite and zircon-type) in $BiVO_4$-YVO_4 system, J. Mater. Chem. C 3 (2015) 2582–2588.